Metabolite elucidation of 2-fluoro-deschloroketamine (2F-DCK) using molecular networking across three complementary in vitro and in vivo models

Thomas Gicquel, Romain Pelletier, Camille Richeval, Alexandr Gish, Florian Hakim, Pierre-Jean Ferron, Vadim Mesli, Delphine Allorge, Isabelle Morel, Jean-Michel Gaulier

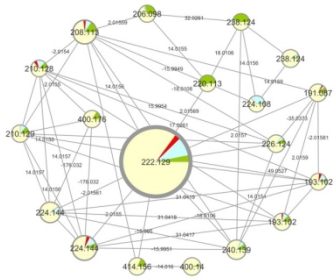

Metabolism elucidation of 2-Fluoro-Deschloroketamine (2F-DCK) using molecular networking in three complementary models (*in vitro, in cadaver*)

Thomas Gicquel, Romain Pelletier, Camille Richeval, Alexandr Gish, Florian Hakim, Vadim Mesli, Delphine Allorge, Isabelle Morel, Jean-michel Gaulier

Molecular network approach (1) allows a 2F-DCK metabolic profile proposal with evaluation using authentic biological *post mortem* samples, and (2) suggests nor-2F-DCK and dihydro-nor-FDCK metabolites as robust, specific and sensitive biomarkers of 2F-DCK use.

Graphical Abstract

318x90mm (150 x 150 DPI)

Metabolite elucidation of 2-Fluoro-Deschloroketamine (2F-DCK) using molecular networking across three complementary *in vitro* and *in vivo* models.

Thomas Gicquel[1,2*], Romain Pelletier[1], Camille Richeval[3,4], Alexandr Gish[3], Florian Hakim[3,4], Pierre-Jean Ferron[2], Vadim Mesli[5], Delphine Allorge[3,4], Isabelle Morel[1,2], Jean-michel Gaulier[3,4]

1 - CHU Rennes, Laboratoire de toxicologie biologique et médicolégale, F-Rennes 35033, France

2 - Univ Rennes, INSERM, INRAE, CHU Rennes, Institut NuMeCan (Nutrition, Metabolismes et Cancer), F-35033 Rennes, France.

3 - CHU Lille, Unité Fonctionnelle de Toxicologie, F-59000 Lille, France

4 - Univ. Lille, ULR 4483 – IMPECS – IMPact de l'Environnement Chimique sur la Santé humaine, F-59000 Lille, France

5 - CHU Lille, Service de Médecine Légale, F-59000 Lille, France

* Correspondence to:

Dr. Thomas Gicquel (ORCID**:** 0000-0002-2354-1884 and Publons: Q-1880-2019) Laboratoire de toxicologie biologique et medico-légale, CHU Pontchaillou, 2 Rue Henri Le Guilloux, 35000 Rennes.

thomas.gicquel@chu-rennes.fr

Abstract

This work first aims to investigate metabolites of 2-Fluoro-Deschloroketamine (2F-DCK), a new arylcyclohexylamine derivatives (a group of dissociative ketamine-based substances) using two *in vitro* experimental approaches, and to compare obtained results by means of molecular networking. Metabolites of 2F-DCK were investigated using both human liver microsomes (HLMs) and hepatic (HepaRG) cell line incubates using molecular networking approach: 2F-DCK pure substance was incubated with HLMs for up to 1h at two concentrations (100 and 500 µM) and with HepaRG cells for two time periods (8h and 24h) at one concentration (20 µM). *In vitro* obtained results were subsequently applied to a 2F-DCK-related fatality case. *In vitro*-produced metabolites were investigated using high-resolution accurate mass spectrometry using Orbitrap mass analyzer technology. Thirteen metabolites were *in vitro* produced and several metabolic pathways can be postulated. Seven additional metabolites were found in *post-mortem* samples (bile and urine) of the case, comprising three phase II metabolites, which appear to be minor *in vivo* metabolites. HLMs and HepaRG cell models appear to be complementary and obtained data allowed the identification of several specific 2F-DCK metabolites in biological samples. In practical terms, observed metabolic ratios suggested that nor-2F-DCK (208.1137 *m/z*) and a hydrogenated metabolite (224.1443 *m/z*) could be proposed as reliable metabolites to be recorded in HRMS libraries in order to improve detection of 2F-DCK use.

Keywords: New Psychoactive Substances, 2F-DCK, Metabolism, molecular networking, microsomes, HepaRG cell line

1. Introduction

New arylcyclohexylamine derivatives (NADs), a group of dissociative substances obtained by slight chemical modification on ketamine scaffold, are worldwide emerging (1,2). A ketamine analogue called "2-Fluoro-Deschloroketamine", "2F-DCK" or "2FK", was recently identified (2–7). A large retrospective study in New York City between 2003 and 2020 showed an increase in traffic fatalities related to ketamine and derivative use, including 2F-DCK (8). 2F-DCK emerged especially in Asian countries where a recent study showed the extent of ketamine and 2F-DCK consumption through their quantification in wastewater from large Chinese cities (9).

Based on its arylcyclohexylamine structure, 2F-DCK is a dissociative anaesthetic N-methyl-D-aspartate (NMDA) glutamatergic receptor antagonist. Nevertheless, there is currently not much information available about the pharmacology, toxicology, and metabolism of 2F-DCK. Furthermore, due to the high frequency of new products in the new psychoactive substances (NPS) area and, consequently, rapidly changing NPS landscape, the detection of NPS-related intoxication case represents a general analytical challenge for toxicologists (10). This issue is linked to several pitfalls including the fact that NPS, such as 2F-DCK, cannot be generally detected using routine laboratory immunoassay tests (*i.e.* screening tests for ecstasy/amphetamine, opiates, cocaine, and cannabis). Moreover, due to their extensive metabolism, the identification of target metabolites is often necessary in order to increase the chance of detecting NPS consumption and to enlarge the detection window in biological matrices from clinical and forensic cases (11–13).

To address this latter problem, NPS metabolism investigations using *in vitro* models, such as pooled human liver microsomes (HLMs) and HepaRG differenciated cell line, are now commonly used (14,15).

In addition, molecular networking (MN) approach offers valuable insights into xenobiotic metabolism by propagating structural information within the network and facilitating sample-to-sample comparison (16). Indeed, this original tool allows organization and visualization of tandem mass spectrometry (MS/MS) data in a graphical representation (17). In this way, MN displays visual representation of chemical similiarity among analytes of an untargeted MS/MS analysis: each node represents an ion and its associated fragmentation spectrum, and the links between different nodes indicate similarities between MS2 spectra. Applied in a multimatrix approach, MN provides a semi-quantitative visualization of molecule repartition in different

samples. MN has already shown its benefit in drug metabolism studies, *in vitro* and *in vivo* (18–21), specifically in NPS intoxication cases (16, 22).

For the first time, we investigated 2F-DCK metabolism using two complementary *in vitro* models, namely HLMs and HepaRG cell line, and compared obtained results using molecular networking. *In vivo* 2F-DCK metabolism was then investigated by the analysis of authentic *post-mortem* biological samples (peripheral blood, urine, bile, vitreous humor) from a recently reported 2F-DCK-related fatal case (5).

2. Material and Methods

Material

β-OH-ethyltheophyllin (internal standard), methyl-clonazepam (internal standard), ammonium formate, formic acid, sulfosalicylic acid dihydrate, alamethicin (*Trichoderma viride*), uridine diphosphate glucuronic acid (UDPGA), glucose-6-phosphate dehydrogenase (G6PD), glucose-6-phosphate (G6P), and 5-sulfosalicylic acid, were all purchased from Sigma-Aldrich (Saint-Quentin-Fallavier, France). Hydrocortisone hemisuccinate was purchased from Serb (Paris, France). Dimethyl sulfoxide (DMSO) was obtained from Sigma-Aldrich (Saint Louis, MO USA). Tetra-sodium salt of a reduced form of nicotinic acid adenine dinucleotide phosphate (NADPH) was purchased from Roche (Mannheim, Germany). Insulin was obtained from Sigma-Aldrich (Saint Louis, MO, USA). William's E medium (Gibco, ThermoFischer Scientific, San Jose, CA) supplemented with 10% fetal bovine serum (Lonza, Verviers, Belgium), penicillin-streptomycin, and L-glutamine were purchased from Life Technologies (Eugene, OR, USA). William's E medium, penicillin–streptomycin, L-glutamine and trypsin were purchased from ThermoFisher Scientific (Saint Aubin, France). 2F-DCK powder was a seized sample of purity greater than 95% (the remaining 5% consisting in inorganic compounds) and in which no significant organic impurity was detected using both liquid chromatography with high-resolution mass spectrometry detection (LC-HRMS) and nuclear magnetic resonance (NMR) methods (5). LC-MS grade water, methanol, and acetonitrile were purchased from Biosolve (Dieuze, France) and all other chemicals such as zinc sulfate were of analytical grade and obtained from common commercial sources. Fetal Bovine Serum (FBS) was purchased from Eurobio (Courtaboeuf, France) and from Hyclone GE Healthcare Life Sciences (Logan, UT USA).

HLM incubates

HLM incubates were prepared as already reported at concentrations usually used (13,14). Once thawed, HLMs (2 mg protein/mL for a final volume of 100 µL) were pre-activated by alamethicin on ice in an intermediate volume of 50 µL in 0.1 M Tris-HCl-$MgCl_2$ (10 mM $MgCl_2$ and 100 mM Tris-HCl solution) at pH 7.4. This mixture was added to a 50 µL-dried residue of two different concentrations of a 2F-DCK solution (100 and 500 µM). Fifty µL of a cofactor mixture (5 mM UDPGA, 1.3 mM NADPH, 3.3 mM G6P and 0.5 U/mL G6PD) in 0.1 M Tris-HCl was then added. The enzymatic reaction was performed at 37 °C for 60 min and stopped by the addition of 100 µL of methanol. Samples were freezed at -20°C until analysis.

HepaRG cell culture and treatment.

The HepaRG cell line was obtained from a liver tumor of a female patient suffering from hepatocarcinoma and was cultured and treated as described previously (21). Briefly, HepaRG cells were seeded at a density of 10^5 cells/well in 96-well plates and cultured during two weeks in culture medium (William's E medium supplemented with 10% FBS, 50 U/mL penicillin, 50 µg/mL streptomycin, 5 µg/mL insulin, 2 mM glutamine, 50 µM sodium hydrocortisone hemisuccinate and 2% DMSO. Cells were then cultured during two additional weeks in the same type of medium supplemented with 2% DMSO to induce cell differentiation into cholangiocyte- and hepatocyte-like cells expressing liver-specific functions. The detection of 2F-DCK and its metabolites was performed using this coculture model. Differentiated HepaRG cells were incubated with 100 µL of 2F-DCK for 8 or 24 hours at 20 µM, a non-cytotoxic concentration. Cell culture supernatants were removed and freezed at -20°C until analysis.

Biological samples

Peripheral blood, bile, vitreous humor, and urine were *post-mortem* samples collected in a fatal self-intoxication case related to 2F-DCK (5). This fatality involved two other NPS (3-MeO-PCE and 5-MeO-DMT) as well as recent use of classical illicit drugs (THC, cocaine, and amphetamine). 2F-DCK concentrations determined by LC-HRMS were 1780, 6100, 12000, and 1500 µg/L in the victim's peripheral blood, urine, bile, and vitreous humor, respectively (5).

Extraction step

Biological, HLM incubates, and HepaRG supernatant samples were extracted as reported previously (19,21). Briefly, 200 µL of each sample were supplemented with 500 µL of methanol containing internal standards (methyl-clonazepam at 1.25 mg/L and β-OH-ethyltheophyllin at 16 mg/L) and then extracted with 300 µL of 0.1 M zinc sulfate solution.

After supernatant evaporation, the residue was dissolved in 200 µL of LC–MS grade water and transferred into chromatographic vials for LC-HRMS analysis.

LC-HRMS/MS analysis

Liquid chromatography-mass spectrometry (LC–MS) analyses were carried out using Orbitrap Q Exactive mass spectrometer coupled to an UltiMate 3000 pump (Thermo Scientific, San Jose, CA). A heated electrospray ionization source (HESI-II) was used for the ionization of the target compounds. Data acquisition, calibration, and instrument control were performed using Xcalibur 2.1 (Thermo Scientific) software. Samples were maintained at 15 °C in the autosampler and quality controls were injected before each analysis. A non-targeted screening LC-HRMS/MS method used for MN building was performed as follows : the mobile phases were composed of ammonium formiate at 2 mM and formic acid 0.1% in water (phase A) and ammonium formiate at 2 mM and formic acid 0.1% in methanol and acetonitrile (50/50) (phase B). LC was performed on a Accucore Phenyl Hexyl (100 × 2.1 mm, 2.6 µm) (Thermo Scientific) using the following gradient elution: initial conditions of 99:1 (A:B) maintained for 1 min, increasing to 1:99 (A:B) for 9 min, followed by a 1.5 min plateau with 1:99 (A:B) and return to initial conditions 99:1 (A:B) for equilibration. This corresponded to a total chromatographic run of 15 min. The flow rate was 500 µL/min, the column temperature was maintained at 40 °C, and the injection volume was 10 µL. For mass spectrometry, the instrument operated in an ESI positive mode and the range for acquisition was 150–450 m/z. Ion precursor selection was performed in the data dependent mode of operation where the most intense ion from the previous scan was selected for fragmentation. Full scan (MS1) data were acquired for each ionization mode at a resolution of 35,000 FWHM, with an AGC target of 1e6 and a maximum injection time of 120 ms. Source parameters were as follows: source voltage + 3.0 kV, sheath gas flow 60 units, auxiliary gas flow 10 units, capillary temperature 320 °C, S-Lens RF level 60 units. MS/MS (MS2) data were acquired at a resolution of 17,500 FWHM with an AGC target of 1e5, maximum injection time was 50 ms, a TopN of 5, an isolation window of 2.0 m/z. The normalized collision energy (NCE) was stepped at 17.5, 35, and 52.5, and the dynamic exclusion time set at 3 s.

Molecular networking generation

Spectral data allowed us to generate MN using semi-quantitative bioinformatic approach. Data processing, visualization, and network analysis, using open source softwares, have been described in details elsewhere (16). Briefly, raw data were converted to an open MS format (.mzXML) with ProteoWizard's MSConvert module (23). The mzXML files were

preprocessed (deconvolution, deisotoping, alignment, gap-filling, filtering) with MZmine 2 software (24). The single .mgf output file was then loaded on the Global Natural Products Social networking (GNPS) web-based platform in order to generate the multi-matrix molecular network (17). Parameters were used at m/z 0.02 for the mass tolerance of precursor and fragment ions used for MS/MS spectral library searching, and m/z 0.02 for the mass tolerance of fragment ions used for MN. Links between nodes were created when the cosine score was greater than 0.7, and the minimum number of common fragment ions shared by two MS/MS spectra was 6. Full data processed through the GNPS platform are accessible through the following links:

Figure 1 : HLM :

https://gnps.ucsd.edu/ProteoSAFe/status.jsp?task=fe6e296f47bb451eadeba745bf7456f2

Figure 2 : HepaRG :

https://gnps.ucsd.edu/ProteoSAFe/status.jsp?task=594d314272a3475289317b4683bc7aca

Figure 3 : Biological sample :

https://gnps.ucsd.edu/ProteoSAFe/status.jsp?task=d9878185cfc642308b46d413c56fb689

The molecular network was visualized using Cytoscape 3.8.0 software (25). The nodes were annotated by spectral matching using SIRIUS 4.0 software (26) and information propagation (identified node can serve as a starting point to identify another node in the same cluster) as already reported (21).

3. Results

2F-DCK metabolism in an acellular model (HLM)

A molecular network was built in order to visualize *in vitro* 2F-DCK metabolism in HLMs (Figure 1A). A cluster containing 9 nodes including a node for 2F-DCK (222.1294 *m/z*) was observed *(the MS2 spectra of 2F-DCK including the structure of the main fragments is provided as supplementary material)*. This node is the central one on the figure. A specific color was assigned to each condition: 2F-DCK was present in the standard solution at 1 mg/L (dark blue), HLM incubation at 100 µM (light blue) and 500 µM (turquoise) (Figure 1B). In the node, respective parts display observed relative analytical signals. Eight other nodes were observed in this cluster and correspond to putative but consistent metabolites produced by HLMs. None of these compounds were found in the standard solution (dark blue). Mass shifts were labelled on the edge links between nodes and permit to identify visually biotransformation reaction (reported in Table 1) by information propagation between the 2F-DCK structurally-closed molecules. Table 1 summarized 2F-DCK and related metabolites

produced by HLMs or HepaRG cells, together with those observed (*in vivo*) in the victim's peripheral blood, urine, bile, and vitreous humour.

Among identified metabolites, nor-2F-DCK (208.1137 *m/z*) was the main metabolite and corresponds to a dealkylated metabolite of 2F-DCK, a loss of methyl corresponding to a mass shift of 14.016 as labelled in the edge between these two nodes. Nodes linked to 2F-DCK and labelled (238.1243 *m/z*) with a mass shift of +15.995 correspond to an oxidation reaction. Hydrogenation of this ion leads to a compound labelled 240.139 *m/z*, such as hydrogenation of nor-2F-DCK (208.1137 *m/z*) leads to compounds labelled 210.1294 *m/z* with a mass shift of 2.0155 *m/z*. At the opposite, dehydrogenation of 2F-DCK (222.1287 *m/z*) produces compounds labelled 224.1443 *m/z.* In this *in vitro* model, 2F-DCK metabolism seems to be more intense at 500 µM considering the appearance of a metabolite (210.1286 *m/z*) which was not produced at 100 µM, larger peak surface for most of the other molecules (238.1243 *m/z*; 224.1443 *m/z;* 240.1393 *m/z*, and 208.1130 *m/z*), and a smaller surface for the parent ion, 2F-DCK. Our data showed also three couples of compounds with the same exact mass but with different retention times (4.5 and 5.0 min for 224.1443 *m/z*, 3.2 and 6 min for 238.1243 *m/z*, 4.1 and 4.5 min for 210.1286 *m/z*, respectively), corresponding to isomers with different fragment ions (Table 1). The nodes labelled 208.1130 and 224.1443 *m/z* (RT=4.5 min) are bigger than the other metabolites suggesting interesting biomarkers. These visual results give a good understanding of the 2F-DCK metabolism pathway and allow to identify the structures of metabolites.

2F-DCK metabolism in a cellular model (HepaRG cells)

In the HepaRG model, we obtained a MN (Figure 2A) exhibited a 2F-DCK-containing cluster (Figure 2B). The 2F-DCK metabolism seems to be more intense when the incubation time is longer (24h in dark pink *versus* 8h in light pink) considering the appearance of a metabolite (238.124 *m/z*) which was not produced after 8h of incubation, a larger peak surface for most of the metabolites, and a smaller peak surface for the parent ion (222.1294 *m/z*). As observed with HLM metabolism, the nodes labelled 208.1137, 210.1286, 224.1443, and 238.1243 *m/z* were present. Here, three nodes corresponding to two exact masses (191.0866 and 193.1024 *m/z* at RT= 4.4 and 5.1 min, respectively) and in agreement with the loss of an amino function were observed in HepaRG cell supernatants but absent in the HLM model. Nor-2F-DCK (208.1130 *m/z*) was the main metabolite produced in HepaRG cell model.

2F-DCK metabolites in authentic biological samples

In order to verify our *in vitro* results, we used *post-mortem* biological samples from a fatality case involving 2F-DCK (5). Metabolites were mainly present in urine (yellow) and bile (green), as shown by metabolic ratio visual observation (Figure 3). M09 and M12 were the most intense metabolites and were observed in all biological matrices analyzed.

We have identified a total of eighteen metabolites in the biological samples that were obviously formed either *via* hydrogenation, *N*-demethylation, hydroxylation, deamination, dehydration, or glucuronidation, or a combination of these reactions, as reported in Figure 4. Metabolites were named from M01 (Hydroxy-2F-DCK at RT=3.2 min and 238.1243 *m/z*) to M20 (Hydroxy-2F-DCK glucuronide at RT=6.1 min and 414.1558 *m/z*) according to their retention time sorting.

Three compounds (M14, M18, and M20) were 2F-DCK glucuroconjugated metabolites and identified in two (bile and urine) of all analysed biological samples at 400.1760, 400.1398, and 414.1558 *m/z*, respectively. Thirteen metabolites identified in HLM incubates and/or in HepaRG supernatants were also detected in the studied biological samples. Metabolic ratios between 2F-DCK and metabolites in biological samples, HLMs, and HepaRG (at 8h and 24h) are reported in Table 1.

4. Discussion

2F-DCK metabolism remains currently poorly described. Davidsen *et al.* (2020) incubated HLMs with 2F-DCK and identified three metabolites (ranked from highest to lowest intensity observed): 208.1130 *m/z* (*N*-demethylation) ; 238.1238 *m/z* (cyclohexanone hydroxylation) and 191.0866 *m/z* (deamination) (3). Tang *et al.* (2020) described a *N*-demethylation reaction producing nor-2F-DCK followed by dehydrogenation (MH+ = 206) or hydroxylation (MH+ = 224) on cyclohexane (4). In the present work, we also identified those previously reported metabolites and named them M09 (nor-2F-DCK at 208.1130 *m/z*), M01, M03, and M19 for the three hydroxy-2F-DCK compounds (238.1238 *m/z*), M05 (206.0975 *m/z*) and M17 (224.1079 *m/z*). Recently, Mestria *et al.* (2021) reported two peaks corresponding to dihydro-nor-2F-DCK (210.1294 *m/z*) and two others corresponding to dihydro-2F-DCK (224.1443 *m/z*) in a *post-mortem* blood sample from a forensic case (7). These compounds have a similar fragmentation pattern than that of metabolites we identified as M07, M13, M15, and M12. This latter metabolite appears to be a major metabolite present in all matrices analysed (*in vitro* and *in vivo*). We also identified 10 other newly described metabolites (Table 1).

Ketamine undergoes extensive hepatic *N*-demethylation to the predominant metabolite norketamine, mainly through CYP2B6 and CYP3A4 pathways, in humans. Norketamine is also further metabolized to hydroxynorketamine by CYP2D6 and CYP2A6 (27). We hypothesized that the same enzymes are involved in the metabolism of 2F-DCK.

N-demethylation of 2F-DCK (nor-2F-DCK or M09) effectively appears to be the main biotransformation reaction regarding our *in vitro* and *in vivo* results. Dehydro-nor-2F-DCK (M05) and hydroxy-nor-2F-DCK (M17) are probably produced by the same metabolization pathways as those of ketamine (28,29). Reduction of the ketone function was observed for 2F-DCK although is has not been described for ketamine in the literature. The presence of glucuronidated metabolites is consistent with the presence of phase I precursor identified by information propagation (+176.032 *m/z*). For example, M14 and M18 are respective glucuronides of M12 and M17.

Even though HepaRG cells are deemed capable of producing phase II metabolites (14,30), no 2F-DCK glucuronides were observed with this *in vitro* model in the present study. Glucuronidation of 2F-DCK phase I metabolites have been already described (27). Here, we identified three 2F-DCK-derived glucuronides in bile and urine (M14, M18, and M20) from a forensic case.

The present study provides new data about the *in vitro* and *in vivo* metabolism of 2F-DCK. The main 2F-DCK metabolites identified are identical between i) an acellular biological model (HLM), ii) a cellular model (HepaRG), and iii) *post-mortem* biological samples from a real case. The observed metabolic ratios suggest that nor-2F-DCK (M09) and dihydro-nor-2F-DCK (M12) could be proposed as reliable metabolites to be recorded in MS/MS or HRMS libraries in order to improve detection of 2F-DCK use by toxicologists.

5. Conclusion

Molecular networks building from high precision spectral data ($[M+H]^+$ and fragments) obtained trough *in vitro* (HLMs and differentiated HepaRG cells) and *in vivo* approaches provide a solution for the identification of unknown metabolites of NPS, and offer a visual representation that facilitates the interpretation and understanding of toxicological results in the context of a death involving NPS. In the present study, this molecular network approach (1) allowed to propose a 2F-DCK metabolic profile in agreement with that observed in authentic biological samples, and (2) strongly suggests that nor-2F-DCK and dihydro-nor-2F-DCK could be used as robust, specific, and sensitive biomarkers of 2F-DCK use.

Figures

Figure 1: Visualization of *in vitro* 2F-DCK metabolism in HLMs using molecular networking. HLMs were incubated with 2F-DCK (100 and 500 µM) during 1h. a) The multimatrix molecular network. Each concentration is depicted in a specific color: 100 µM (light blue) and 500 µM (turquoise) and standard solution (dark blue). b) Details of the specific 2F-DCK-containing cluster. Nodes are labelled with the exact protonated mass (*m/z*) and the links are labelled with the exact mass shift. Proposed metabolites of 2F-DCK structure are linked to the corresponding nodes (# exact position of the chemical function is not determined).

Figure 2 : Visualization of *in vitro* 2F-DCK metabolism in HepaRG cells using molecular networking. Differentiated HepaRG cells were incubated with 2F-DCK (20 µM) during 8h (light pink) and 24h (pink). a) The multimatrix molecular network. b) Details of the specific 2F-DCK-containing cluster. Nodes are labelled with the exact protonated mass (*m/z*) and the links are labelled with the exact mass shift. Proposed metabolites of 2F-DCK structure are linked to the corresponding nodes (# exact position of the chemical function is not determined).

Figure 3: Visualization of *in vivo* 2F-DCK metabolism in an authentic case in the 2F-DCK-containing cluster. Nodes are labelled with the exact protonated mass (*m/z*) and the links are labelled with the exact mass shift. Four biological matrices are studied : blood (red), urine (yellow), vitreous humor (blue), and bile (green). Proposed metabolites of 2F-DCK structure are linked to the corresponding nodes (# exact position of the chemical function is not determined).

Figure 4: Proposed metabolites of 2F-DCK structure and postulated biotransformation combining both *in vitro* and *in vivo* studies (# exact position of the chemical function is not determined).

Tables

Table 1: Metabolites of 2F-DCK sorted by retention times (RT), the underlying name or biotransformation, formula, accurate mass of the precursor ions $[M+H]^+$, mass error (Δppm), main observed MS/MS product ions and metabolic ratio in the different matrices analysed [chromatographic peak area of the molecular ion $[M+H]^+$ of the compound of interest normalized to chromatographic peak area (100 %) of 2F-DCK]. Better biomarkers are in bold style.

REFERENCES

1. European Monitoring Centre for Drugs and Drug Addiction. European Drug Report 2020: trends and developments. [Internet]. LU: Publications Office; 2020 [cited 2021 Jun 10]. Available from: https://data.europa.eu/doi/10.2810/420678
2. Li C, Lai CK, Tang MHY, Chan CCK, Chong YK, Mak TWL. Ketamine analogues multiplying in Hong Kong. *Hong Kong Med J.* 2019;25(2):169.
3. Davidsen AB, Mardal M, Holm NB, Andreasen AK, Johansen SS, Noble C, et al. Ketamine analogues: Comparative toxicokinetic in vitro-in vivo extrapolation and quantification of 2-fluorodeschloroketamine in forensic blood and hair samples. *J Pharm Biomed Anal.* 2020;180:113049.
4. Tang MHY, Li TC, Lai CK, Chong YK, Ching CK, Mak TWL. Emergence of new psychoactive substance 2-fluorodeschloroketamine: Toxicology and urinary analysis in a cluster of patients exposed to ketamine and multiple analogues. *Forensic Sci Int.* 2020;312:110327.
5. Gicquel T, Richeval C, Mesli V, Gish A, Hakim F, Pelletier R, et al. Fatal intoxication related to two new arylcyclohexylamine derivatives (2F-DCK and 3-MeO-PCE). *Forensic Sci Int.* 2021;324:110852.
6. Wallach J, Brandt SD. 1,2-Diarylethylamine- and Ketamine-Based New Psychoactive Substances. In: Maurer HH, Brandt SD, editors. New Psychoactive Substances : Pharmacology, Clinical, Forensic and Analytical Toxicology [Internet]. Cham: Springer International Publishing; 2018 [cited 2020 Nov 22]. p. 305–52. (Handbook of Experimental Pharmacology). Available from: https://doi.org/10.1007/164_2018_148
7. Mestria S, Odoardi S, Biosa G, Valentini V, Di Masi G, Cittadini F, et al. Method development for the identification of methoxpropamine, 2-fluoro-deschloroketamine and deschloroketamine and their main metabolites in blood and hair and forensic application. *Forensic Sci Int.* 2021;323:110817.
8. Arango E, Toriello A, Rosario Z, Cooper G. Increasing Prevalence of Ketamine in Drivers in New York City Including the Identification of 2-Fluoro-Deschloroketamine. *J Anal Toxicol.* 2021; bkab057. doi: 10.1093/jat/bkab057.
9. Shao X-T, Yu H, Lin J-G, Kong X-P, Wang Z, Wang D-G. Presence of the ketamine analog of 2-fluorodeschloroketamine residues in wastewater. *Drug Test Anal.* 2021; doi: 10.1002/dta.3098.
10. Huestis MA, Brandt SD, Rana S, Auwärter V, Baumann MH. Impact of Novel Psychoactive Substances on Clinical and Forensic Toxicology and Global Public Health. *Clin Chem.* 2017;63(10):1564–9.
11. Grapp M, Kaufmann C, Schwelm HM, Neukamm MA, Blaschke S, Eidizadeh A. Intoxication cases associated with the novel designer drug 3',4'-methylenedioxy-α-pyrrolidinohexanophenone and studies on its human metabolism using high-resolution mass spectrometry. *Drug Test Anal.* 2020;12(9):1320–35.
12. Salle S, Bodeau S, Dhersin A, Ferdonnet M, Gonçalves R, Lenski M, et al. Novel synthetic opioids: A review of the literature. *Toxicol Anal Clin.* 2019;31(4):298–316.
13. Richeval C, Gaulier J-M, Romeuf L, Allorge D, Gaillard Y. Case report: relevance of metabolite identification to detect new synthetic opioid intoxications illustrated by U-47700. *Int J Legal Med.* 2019;133(1):133–42.
14. Richeval C, Gicquel T, Hugbart C, Le Dare B, Allorge D, Morel I, et al. In vitro Characterization of NPS Metabolites Produced by Human Liver Microsomes and the HepaRG Cell Line Using Liquid Chromatographyhigh Resolution Mass Spectrometry (LC-HRMS) Analysis: Application to Furanyl Fentanyl. *Curr Pharm Biotechnol.* 2017;18(10):806–14.
15. Wagmann L, Frankenfeld F, Park YM, Herrmann J, Fischmann S, Westphal F, et al.

How to Study the Metabolism of New Psychoactive Substances for the Purpose of Toxicological Screenings-A Follow-Up Study Comparing Pooled Human Liver S9, HepaRG Cells, and Zebrafish Larvae. *Front Chem.* 2020;8:539.
16. Allard S, Allard P-M, Morel I, Gicquel T. Application of a molecular networking approach for clinical and forensic toxicology exemplified in three cases involving 3-MeO-PCP, doxylamine, and chlormequat. *Drug Test Anal.* 2019;11(5):669–77.
17. Wang M, Carver JJ, Phelan VV, Sanchez LM, Garg N, Peng Y, et al. Sharing and community curation of mass spectrometry data with Global Natural Products Social Molecular Networking. *Nat Biotechnol.* 2016;34(8):828–37.
18. Allard S, Le Daré B, Allard P-M, Morel I, Gicquel T. Comparative molecular networking analysis of a Rauwolfia plant powder and biological matrices in a fatal ingestion case. *Forensic Toxicol.* 2020;38(2):447–54.
19. Le Daré B, Allard S, Bouvet R, Baert A, Allard P-M, Morel I, et al. A case of fatal acebutolol poisoning: an illustration of the potential of molecular networking. *Int J Legal Med.* 2020;134(1):251–6.
20. Le Daré B, Ferron P-J, Couette A, Ribault C, Morel I, Gicquel T. In vivo and in vitro α-amanitin metabolism studies using molecular networking. *Toxicol Lett.* 2021;346:1–6.
21. Le Daré B, Ferron P-J, Allard P-M, Clément B, Morel I, Gicquel T. New insights into quetiapine metabolism using molecular networking. *Sci Rep.* 2020;10(1):19921.
22. Pelletier R, Le Daré B, Grandin L, Couette A, Ferron P-J, Morel I, et al. New psychoactive substance cocktail in an intensive care intoxication case elucidated by molecular networking. *Clin Toxicol (Phila).* 2021;1–4. doi: 10.1080/15563650.2021.1931693.
23. Kessner D, Chambers M, Burke R, Agus D, Mallick P. ProteoWizard: open source software for rapid proteomics tools development. *Bioinformatics.* 2008;24(21):2534–6.
24. Olivon F, Grelier G, Roussi F, Litaudon M, Touboul D. MZmine 2 Data-Preprocessing To Enhance Molecular Networking Reliability. *Anal Chem.* 2017;89(15):7836–40.
25. Shannon P, Markiel A, Ozier O, Baliga NS, Wang JT, Ramage D, et al. Cytoscape: a software environment for integrated models of biomolecular interaction networks. *Genome Res.* 2003;13(11):2498–504.
26. Dührkop K, Fleischauer M, Ludwig M, Aksenov AA, Melnik AV, Meusel M, et al. SIRIUS 4: a rapid tool for turning tandem mass spectra into metabolite structure information. *Nat Methods.* 2019;16(4):299–302.
27. Dinis-Oliveira RJ. Metabolism and metabolomics of ketamine: a toxicological approach. *Forensic Sci Res.* 2017;2(1):2–10.
28. Desta Z, Moaddel R, Ogburn ET, Xu C, Ramamoorthy A, Venkata SLV, et al. Stereoselective and regiospecific hydroxylation of ketamine and norketamine. *Xenobiotica* 2012;42(11):1076–87.
29. Rao LK, Flaker AM, Friedel CC, Kharasch ED. Role of Cytochrome P4502B6 Polymorphisms in Ketamine Metabolism and Clearance. *Anesthesiology.* 2016;125(6):1103–12.
30. Hugbart C, Verres Y, Le Daré B, Bucher S, Vène E, Bodin A, et al. Non-oxidative ethanol metabolism in human hepatic cells in vitro: Involvement of uridine diphospho-glucuronosyltransferase 1A9 in ethylglucuronide production. *Toxicol In Vitro.* 2020;66:104842. doi: 10.101*6/j.tiv.2020.104842*

	Name	Formula	RT (min)	$[M+H]^+$ observed	$[M+H]^+$ expected	Δppm	Main observed fragment ions	HLM (%)	HepaRG (%)		Blood (%)	Urine (%)	Vitreous humor (%)	Bile (%)
									8h	24h				
Parent	**2F-DCK**	**$C_{13}H_{16}FNO$**	4.6	222.1286	222.1294	-3,2	109; 163; 191	100	100	100	100	100	100	100
M01	Hydroxy-2F-DCK (isomer 1)	$C_{13}H_{16}FNO_2$	3.2	238.1238	238.1243	-2,2	109; 135; 161; 179	2	<1	<1	nd	3	2	2
M02	Dihydro-hydroxy-nor-2F-DCK	$C_{12}H_{16}FNO_2$	3.3	226.1238	226.1243	-2,4	109; 123; 163; 191	nd	nd	nd	<1	3	2	7
M03	Hydroxy-2F-DCK (isomer 2)	$C_{13}H_{16}FNO_2$	3.7	238.1238	238.1243	-2,2	123; 161; 189	nd	<1	<1	nd	1	<1	20
M04	Hydroxy-hydro-2F-DCK	$C_{13}H_{18}FNO_2$	3.8	240.1393	240.1399	-2,8	109; 123; 163; 191	2	nd	nd	<1	6	5	20
M05	Dehydro-nor-2F-DCK	$C_{12}H_{12}FNO$	4.0	206.0975	206.0981	-3,0	146; 161; 189	nd	nd	nd	<1	2	<1	17
M06	Dihydro-deamino-nor-2F-DCK (isomer 1)	$C_{12}H_{13}FO$	4.1	193.1024	193.1028	-2,4	109; 125; 175	nd	<1	<1	2	2	3	7
M07	Dihydro-nor-2F-DCK (isomer 1)	$C_{12}H_{16}FNO$	4.1	210.1286	210.1294	-3,9	109; 125; 175; 193	<1	<1	<1	<1	2	2	10
M08	Dehydro-2F-DCK	$C_{13}H_{14}FNO$	4.3	220.1129	220.1137	-3,9	146; 161; 189	nd	nd	nd	<1	<1	<1	21
M09	**Nor-2F-DCK**	**$C_{12}H_{14}FNO$**	4.4	208.1130	208.1137	-3,7	109; 163; 191	15	10	17	21	14	15	81
M10	Dihydro-deamino-nor-2F-DCK (isomer 2)	$C_{12}H_{13}FO$	4.4	193.1024	193.1028	-2,4	109; 125; 175	nd	<1	<1	2	1	2	2
M11	deamino-2F-DCK	$C_{12}H_{11}FO$	4.4	191.0866	191.0872	-3,2	109; 163	nd	2	3	2	2	1	9
M12	**Dihydro-2F-DCK (isomer 1)**	**$C_{13}H_{18}FNO$**	4.5	224.1442	224.1451	-3,9	109; 135; 179; 161	16	1	2	29	16	21	35
M13	Dihydro-deamino-nor-2F-DCK (isomer 2)	$C_{12}H_{16}FNO$	4.5	210.1286	210.1294	-3,9	109; 125; 175; 193	<1	nd	nd	2	<1	2	4
M14	Dihydro-2F-DCK-glucuronide	$C_{19}H_{26}FNO_7$	4.8	400.1760	400.1771	-2,9	85; 109; 193	nd	nd	nd	nd	nd	2	10
M15	Dihydro-2F-DCK (isomer 2)	$C_{13}H_{18}FNO$	5.0	224.1442	224.1451	-3,9	109; 125; 175; 193	6	1	3	1	8	8	1
M16	Dihydro-deamino-nor-2F-DCK (isomer 3)	$C_{12}H_{13}FO$	5.1	193.1024	193.1028	-2,4	109; 125; 175	nd	<1	<1	nd	nd	nd	nd
M17	Hydroxy-nor-2F-DCK	$C_{12}H_{14}FNO_2$	5.5	224.1079	224.1086	-3,5	109; 178; 206	nd	nd	nd	nd	<1	<1	nd
M18	Hydroxy-nor-2F-DCK glucuronide	$C_{18}H_{22}FNO_8$	5.7	400.1398	400.1407	-2,4	109; 178; 206	nd	nd	nd	nd	3	nd	3
M19	Hydroxy-2F-DCK (isomer 3)	$C_{13}H_{16}FNO_2$	6.0	238.1238	238.1243	-2,2	109; 163; 191	<1	nd	<1	nd	nd	nd	nd
M20	Hydroxy-2F-DCK glucuronide	$C_{19}H_{24}FNO_8$	6.1	414.1558	414.1564	-1,5	109; 163; 191	nd	nd	nd	nd	2	nd	11

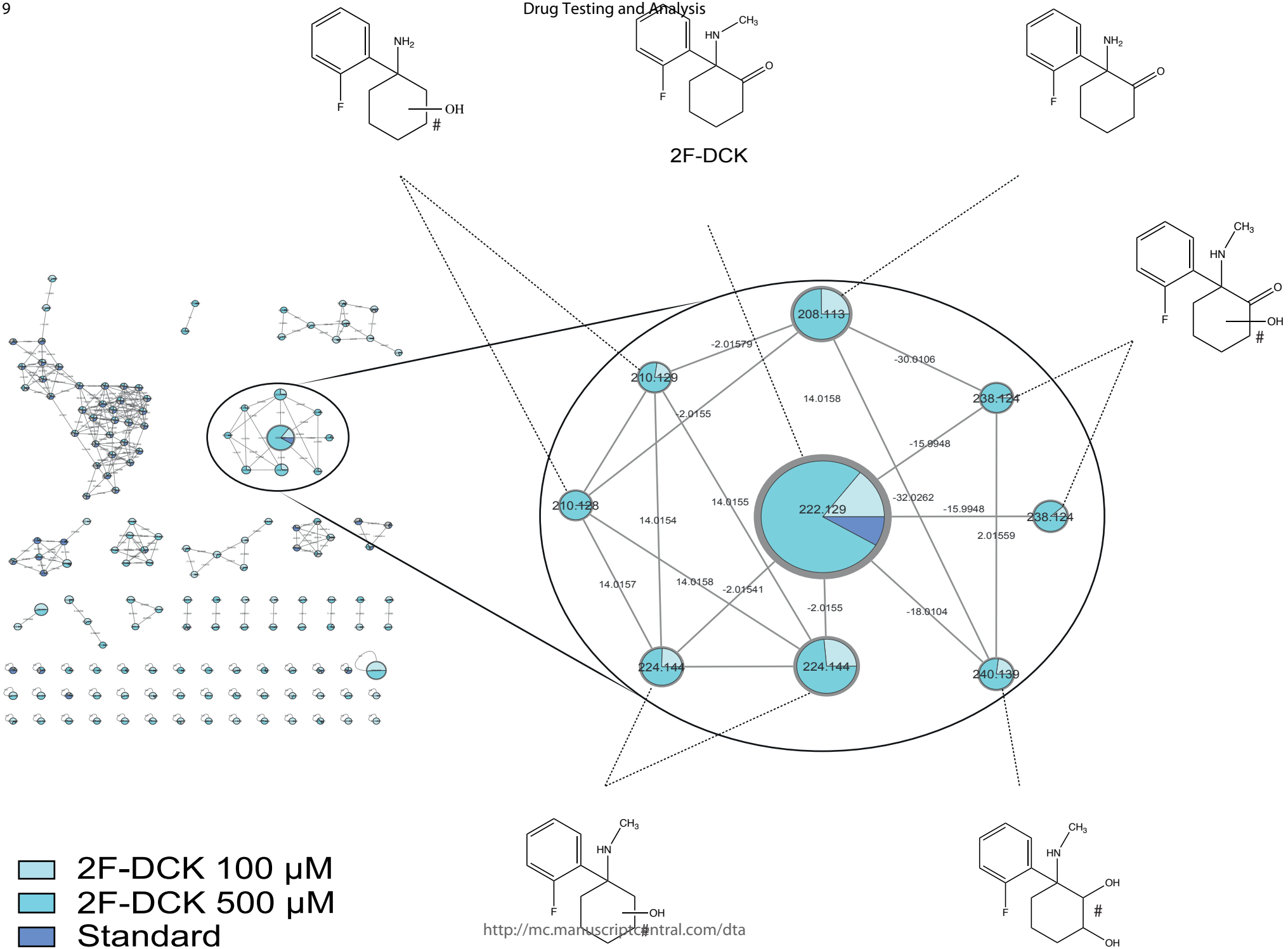
2F-DCK
208.113
210.129
238.124
210.128
222.129
238.124
224.144
224.144
240.139
-2.01579
-30.0106
14.0158
-2.0155
-15.9948
-32.0262
-15.9948
14.0155
14.0154
2.01559
14.0157
14.0158
-2.01541
-2.0155
-18.0104
2F-DCK 100 µM
2F-DCK 500 µM
Standard

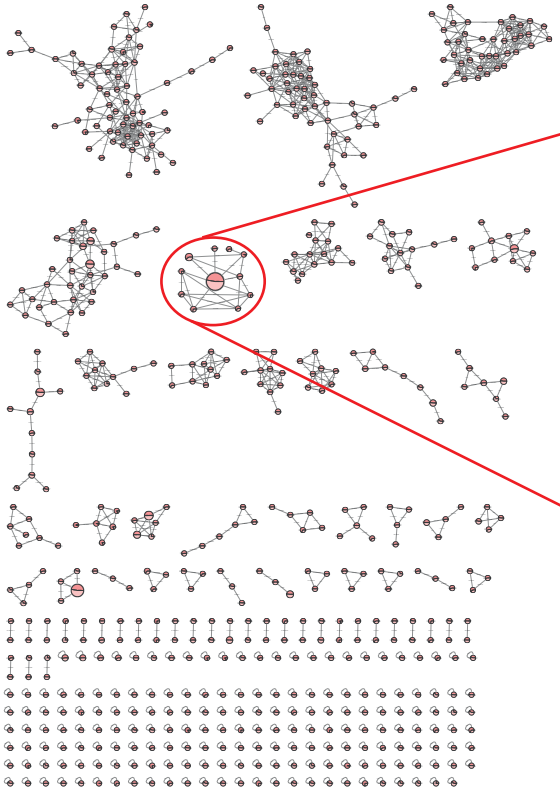

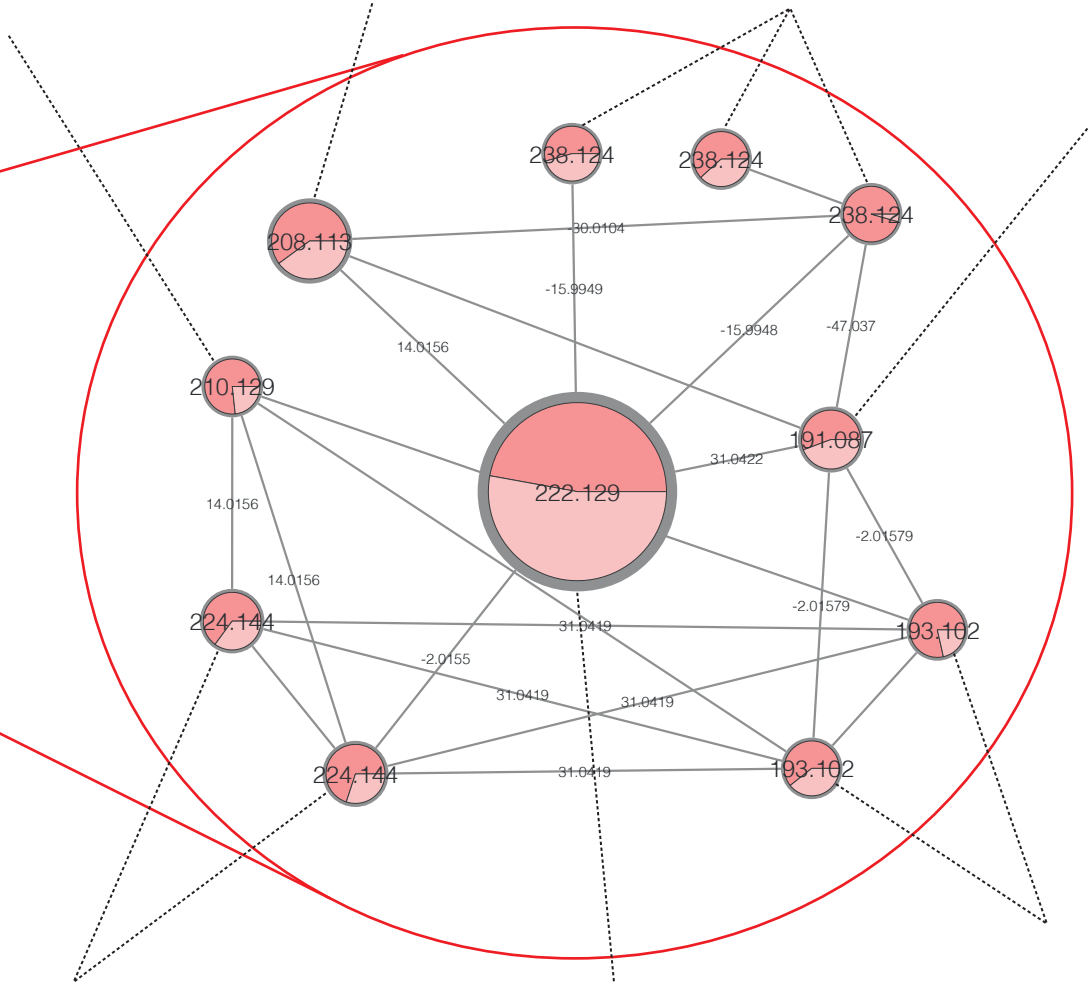

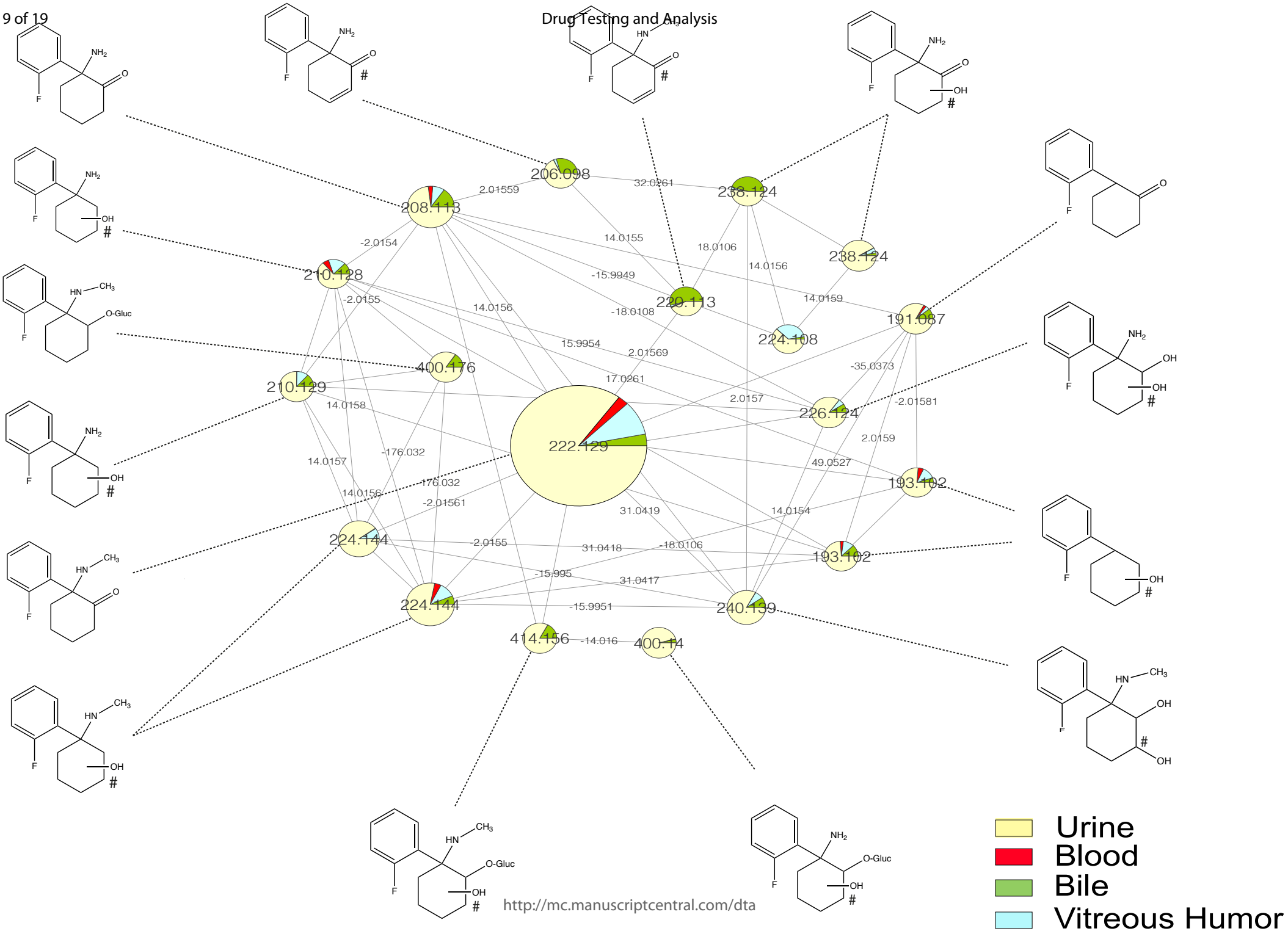
206.098
238.124
208.113
238.124
210.128
220.113
224.108
191.087
400.176
210.129
222.129
226.124
193.102
224.144
193.102
224.144
240.139
414.156
400.14
2.01559
32.0261
-2.0154
14.0155
18.0106
14.0156
-15.9949
-2.0155
14.0156
-18.0108
14.0159
15.9954
2.01569
-35.0373
17.0261
14.0158
2.0157
-2.01581
-176.032
14.0157
2.0159
49.0527
176.032
14.0156
-2.01561
31.0419
14.0154
-2.0155
31.0418
-18.0106
-15.995
31.0417
-15.9951
-14.016
Urine
Blood
Bile
Vitreous Humor

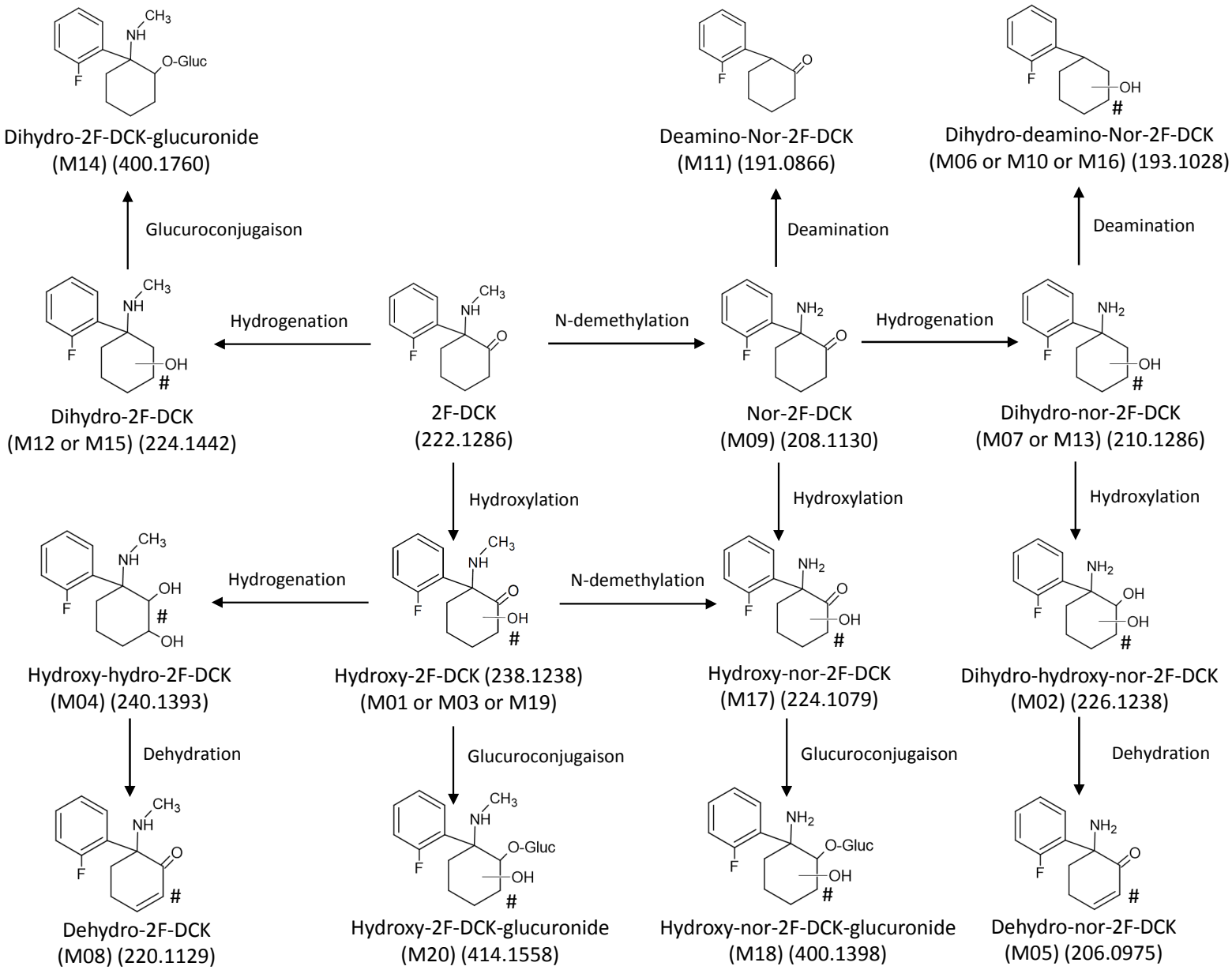
Dihydro-2F-DCK-glucuronide
(M14) (400.1760)
Glucuroconjugaison
Deamino-Nor-2F-DCK
(M11) (191.0866)
Deamination
Dihydro-deamino-Nor-2F-DCK
(M06 or M10 or M16) (193.1028)
Deamination
Hydrogenation
N-demethylation
Hydrogenation
Dihydro-2F-DCK
(M12 or M15) (224.1442)
2F-DCK
(222.1286)
Nor-2F-DCK
(M09) (208.1130)
Dihydro-nor-2F-DCK
(M07 or M13) (210.1286)
Hydroxylation
Hydroxylation
Hydroxylation
Hydrogenation
N-demethylation
Hydroxy-hydro-2F-DCK
(M04) (240.1393)
Hydroxy-2F-DCK (238.1238)
(M01 or M03 or M19)
Hydroxy-nor-2F-DCK
(M17) (224.1079)
Dihydro-hydroxy-nor-2F-DCK
(M02) (226.1238)
Dehydration
Glucuroconjugaison
Glucuroconjugaison
Dehydration
Dehydro-2F-DCK
(M08) (220.1129)
Hydroxy-2F-DCK-glucuronide
(M20) (414.1558)
Hydroxy-nor-2F-DCK-glucuronide
(M18) (400.1398)
Dehydro-nor-2F-DCK
(M05) (206.0975)